Inorganica Chimica Acta 429 (2015) 174–182

Contents lists available at ScienceDirect

Inorganica Chimica Acta

journal homepage: www.elsevier.com/locate/ica

Exploring the photo-stability of the $\{Ru(py)_4\}^{2+}$ fragment

Juan P. Marcolongo [a], Thomas Weyhermüller [b], Leonardo D. Slep [a,*]

[a] Departamento de Química Inorgánica, Analítica y Química Física, Facultad de Ciencias Exactas y Naturales, and INQUIMAE Universidad de Buenos Aires – CONICET, Pabellón 2, 3er piso, Ciudad Universitaria, C1428EHA Ciudad Autónoma de Buenos Aires, Argentina
[b] Max-Planck-Institut für Chemische Energiekonversion, Stiftstraße 34-36, D-45470 Mülheim am der Ruhr, Germany

ARTICLE INFO

Article history:
Received 18 September 2014
Received in revised form 25 November 2014
Accepted 27 December 2014
Available online 14 February 2015

Keywords:
Ruthenium
Building blocks
Molecular devices
Photochemistry

ABSTRACT

Mononuclear Ru(II) tetrakis-pyridine species of general formula *trans*-$[(Cl)Ru(py)_4(X)]^{n+}$ (X = Cl^-, MeCN and CO) are thermally inert toward ligand exchange reactions at room temperature, but undergo substitution under photolysis conditions. The carbonyl derivative *trans*-$[(Cl)Ru^{II}(py)_4(CO)]^+$ was specifically synthesized for this report by the direct reaction between *trans*-$[(Cl)Ru^{II}(py)_4(Solv)]^+$ and CO in acetone and isolated as a PF_6^- salt. Stationary photolysis experiments in MeCN allowed recording changes in the absorption profiles along time providing quantitative values for the quantum yields of the different photo-processes, which involve the consecutive loss of CO, MeCN or pyridine ligands. There is no evidence of photo-release of a chloride anion in none of the molecules under study. For X = CO and MeCN the photo-release of X is favored over the substitution of a pyridine molecule.

1. Introduction

Coordination compounds have been vastly employed in the preparation of supramolecular assemblies. Metal containing fragments provide an extensive variety of structures and functions that make them attractive in the field. Particularly the $\{Ru(py)_4\}^{2+}$ fragment has been involved in the preparation of systems with diverse degree of complexity, from of mononuclear [1–16] to dinuclear [17,18] and oligonuclear species [19–24]. With only very few documented exceptions [17], the $\{Ru(py)_4\}^{2+}$ fragments adopt the well known paddlewheel arrangement of the equatorial pyridine ligands, leaving the two extra coordination sites in *trans*-configuration. This structural feature allowed overcoming the constrains imposed by other Ru containing (poly)pyridine moieties for the construction of oligonuclear assemblies. The $\{Ru(py)_4\}^{2+}$ moiety is also known to be thermally robust, and for that reason has been suggested as the ideal building block to assemble molecular devices.

The incorporation of this fragment into molecular devices depends on the desired substitution pattern: for symmetrically disubstituted tetrapyridine derivatives the starting material of choice is usually *trans*-$(Cl)_2Ru^{II}(py)_4$ (**[Ru-Cl]^0**). The preparation of asymmetrically disusbstituted species usually involves the consecutive replacement of the axial ligands in the precursor species *trans*-$[(Cl)Ru(py)_4(NO)]^{2+}$ (**[Ru-NO]$^{2+}$**) [23]. The controlled replacement is possible because of the electrophilic reactivity of the $\{Ru\text{-}NO\}^6$ moiety [25] that allows converting the otherwise substitutionally inert nitrosyl-derivative into a more labile nitro-compound by reaction with OH^- in aqueous medium.

The consensus is that, unlike other Ru(poly)pyridine systems [26], the $\{Ru(py)_4\}^{2+}$ moiety is photochemically stable and that the identity and stereochemistry of the coordination sphere remains unaltered under irradiation. This widespread belief is most probably due to the fact that the tetrapyridine chromophore shows absorption features which are blue shifted if compared to the polypyridinic system and is actually not well supported by experimental information. To our knowledge, there is a single report concerning the photochemistry in solution of this fragment, which explores the phtodetachment of NO from *trans*-$[(Cl)Ru(py)_4(NO)]^{2+}$ and the dinulcear species *trans*-$[(NC)Ru(py)_4(\mu\text{-}CN)Ru(py)_4(NO)]^{3+}$ [27]. The former releases a neutral nitric oxide molecule yielding an M(III) solvento species, as in Eq. (1) with $\phi_{NO} = (1.63 \pm 0.04) \times 10^{-3}$ mol einstein^{-1}, while the latter is much less reactive due to the electronic nature of the lowest energy triplet excited state.

$$trans\text{-}[(Cl)Ru(py)_4(NO)]^{2+} \xrightarrow[+H_2O]{h\nu} trans\text{-}[(Cl)Ru(py)_4(H_2O)]^{2+} + NO^o \quad (1)$$

Due to the still ongoing interest in employing this fragment, we decided to explore the photoreactivity of several simple mononuclear compounds holding axial ligands that span a wide range in terms of donor/acceptor properties. The compounds of choice respond to the general formula *trans*-$[(Cl)Ru(py)_4(X)]^{n+}$:

* Corresponding author.

http://dx.doi.org/10.1016/j.ica.2014.12.039
0020-1693/

trans-$(Cl)_2Ru(py)_4$, *trans*-$[(Cl)Ru(py)_4(MeCN)]^+$, the already mentioned *trans*-$[(Cl)Ru(py)_4(NO)]^{2+}$ and its carbonyl-holding isoelectronic analog *trans*-$[(Cl)Ru(py)_4(CO)]^+$. We report here the preparation of the latter, together with a comparative structural and spectroscopic characterization, of the series to finally explore the photo-reactivity of the species attempting to provide a unified picture which could help to rationalize observations.

2. Results and discussion

2.1. Synthesis, structure and basic characterization

The usual strategy to yield asymmetrically disubstituted tetrapyridine species relies on the differential reactivity of both axial substituents in *trans*-$[(Cl)Ru^{II}(py)_4(NO)]^{2+}$ to yield an intermediate solvento complex where the L group could be readily incorporated:

$$trans\text{-}[(Cl)Ru^{II}(py)_4(NO)]^{2+} \xrightarrow[\text{Acetone}]{NaN_3} trans\text{-}[(Cl)Ru^{II}(py)_4(Solv)]^{+} \quad (2)$$

$$trans\text{-}[(Cl)Ru^{II}(py)_4(Solv)]^{+} \xrightarrow[\text{Acetone}]{L} trans\text{-}[(Cl)Ru^{II}(py)_4(L)]^{+} \quad (3)$$

This path proved to be successful in the preparation of several $\{Ru(py)_4\}^{2+}$ holding compounds, particularly *trans*-$[(Cl)Ru(py)_4(MeCN)]^+$, and now *trans*-$[(Cl)Ru(py)_4(CO)]^+$ (**[Ru-CO]$^+$**). The insertion of carbon monoxide in the coordination sphere proceeded smoothly under an atmosphere of CO (1 bar) at room temperature, and the monocationic product **[Ru-CO]$^+$** could be easily isolated by consecutive addition of PF_6^- and diethyl ether (Et_2O) to yield **[Ru-CO]**(PF_6). Single crystals were grown by slow diffusion of Et_2O into a MeCN solution of the compound.

The new complex crystallizes in the tetragonal space group *P4/n* containing two formula units per unit cell (see Table 1). The X-ray structure determination reveals the presence of a **[Ru-CO]$^+$** cationic unit and a well separated PF_6^- counterion. Cation and anion each reside on a crystallographic fourfold rotation axes. The cation is packed with its fourfold Cl–Ru–CO molecular axis in a head to tail type fashion along the crystallographic fourfold-axis (Fig. 1). The crystallographic inversion center results in anti-parallel chains of **[Ru-CO]$^+$** units distant at 8.06 Å. The same arrangement holds for the F–P–F axes of the PF_6^- molecules, which are arranged in columns distant at 8.060(1) Å from each other and 5.699(1) Å from the closest **[Ru-CO]$^+$** columnar arrangement.

The Ru center is located above (0.0076(2) Å) the 0.07 Å above the plane defined by the N-atoms of the four pyridine ligands. A neutral CO molecule and a chloride anion located above and below the equatorial plane defined by the four pyridine ligands complete the pseudooctahedral coordination environment (Table 2). The conformation of the equatorial ligands preserves the usual propeller like configuration observed for other tetrakis-pyridine Ru(II) compounds. The pyridine tilting angle approaches 46°, as observed in similar compounds [9,28,29]. The Ru–N1 bond length is 2.1056(13) Å, coincident within the experimental uncertainty with the one reported for *trans*-$[(Cl)Ru^{II}(py)_4(NO)](PF_6)_2{\cdot}½(H_2O)$ (**[Ru-NO]**$(PF_6)_2{\cdot}½(H_2O)$; average of 2.109(8) Å) [9] and slightly longer than the reported value for *trans*-$(Cl)_2Ru(py)_4$ (**[Ru-Cl]^0**; 2.073(3) Å) [28]. The. The Ru–Cl, Ru–C and C–O bond lengths are at 2.4414(7) Å, 1.849(4) Å and 1.143(5) Å, respectively. The Ru–Cl bond is comparable (though slightly shorter) to the one reported for **[Ru-Cl]^0** (2.406(1) Å) [28] and significantly longer than the one in **[Ru-NO]$^{2+}$** (2.315(3) Å) [9]. The latter is actually close to the Ru(III)–Cl bond reported in the one-electron oxidized species **[Ru-Cl]$^+$**, 2.326(4) Å [29].

The in vacuo geometries predicted by DFT calculations for all the compounds studied here agree well with the experimental findings (see Table 3 and Fig. 2).

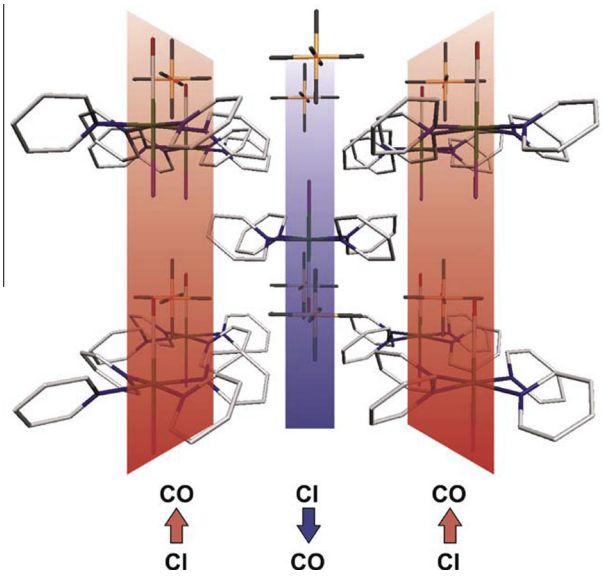

Fig. 1. Packing diagram of **[Ru-CO]$^+$** in crystals of **[Ru-CO]**PF_6, showing the alignment of the Cl–Ru–CO molecular axes.

Table 1
Crystallographic data for *trans*-$[(Cl)Ru(py)_4(CO)](PF_6)$.

	trans-$[(Cl)Ru(py)_4(CO)](PF_6)$
Formula	$C_{21}H_{20}ClF_6N_4OPRu$
Mr	625.90
Crystal system	tetragonal
Space group	*P4/n* N° 85
α (Å)	11.3979(8)
χ (Å)	9.1023(6)
V (Å^3)	1182.50(18)
Z	2
D_{calc} (Mg m^{-3})	1.758
T (K)	100(2)
μ (mm^{-1})	0.914
Data/parameters	2610/83
θ-range (°)	3.376–34.980
Collected/unique reflections	23 034/2610
R_1, wR_2 ($I > 2\sigma$ (I))[a]	0.0314, 0.0765
R_1, wR_2 (all data)	0.0383, 0.0809
Goodness-of-fit (GOF) on *F2*	1.058

[a] *R*-indices defined as: $R_1 = \sum||F_o| - |F_c||/\sum|F_o|$, $wR_2 = [\sum w(F_o^2 - F_c^2)^2/\sum w(F_o^2)^2]^{1/2}$.

Table 2
Selected bond lengths and angles for *trans*-$[(Cl)Ru(py)_4(CO)](PF_6)$.

Bond lengths (Å)	
Ru1–Cl1	2.4414(7)
Ru1–C11	1.849(4)
Ru1–N1	2.1056(13)
N1–C2	1.3522(19)
N1–C6	1.3535(19)
C2–C3	1.384(2)
C3–C4	1.388(2)
C4–C5	1.386(3)
C5–C6	1.387(2)
C11–O12	1.143(5)
Angles (°)	
O12–C11–Ru1	180.0
C11–Ru1–Cl1	180.0
N1–Ru1–Cl1	88.11(3)
C11–Ru1–N1	91.89(3)
Cl1–Ru1–N1–C6	46.4(1)
N1–Ru1–N1′	89.937(3)

Table 3
Selected bond lengths and angles for the DFT optimized structures of **[Ru-CO]$^+$** and related species.

	[Ru-CO]$^+$ (vacuo)	**[Ru-CO]$^+$** (MeCN)	**[Ru-CO]$^{2+}$** (MeCN)	**[Ru-NO]$^{2+}$** (MeCN)	**[Ru-Cl]^0** (MeCN)	**[Ru-Cl]$^+$** (MeCN)	**[Ru-MeCN]$^+$** (MeCN)	**[Ru-MeCN]$^{2+}$** (MeCN)
d(Ru-X)/Å	1.86	1.84	1.92	1.77	–	–	2.01	2.08
d(X-O)/Å	1.19	1.19	1.16	1.18	–	–	–	–
d(Ru-N_{py})/Å	2.14	2.14	2.12	2.14	2.11	2.13	2.12	2.12
d(Ru-Cl)/Å	2.52	2.56	2.49	2.41	2.55	2.45	2.53	2.39
d(N-C)/Å	–	–	–	–	–	–	1.17	1.17
θ(Ru-X-O)/°	179.97	179.95	179.92	179.62	–	–	179.89(Ru-N-C)	179.98(Ru-N-C)
θ(Cl-Ru-X)/°	179.98	179.90	179.93	179.69	179.93	179.87	179.88	179.91
θ(C_2-N_1-N_1-C_2)/°	103.39	94.52	86.16	89.98	88.78	83.64	82.84	86.19
θ(X-Ru-N_1-C_6)/°	40.50	45.36	38.63	43.81	41.86	44.05	41.64	43.06
θ(N_1-Ru-$N'_{1\,perp}$)/°	89.95	89.96	90.16	90.02	90.07	91.53	91.70	91.32

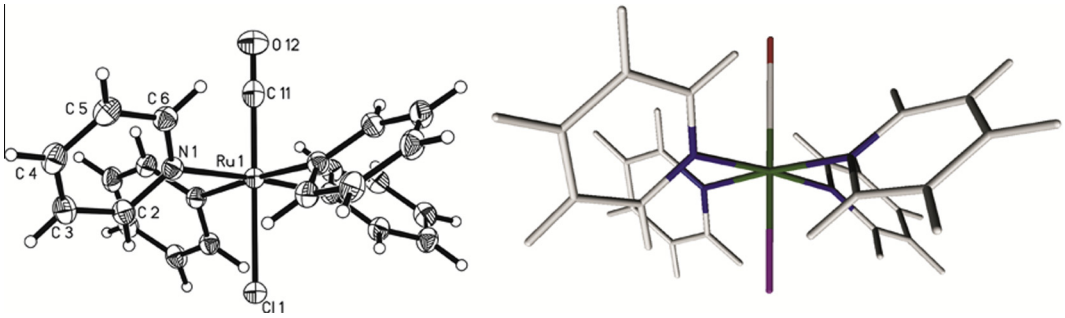

Fig. 2. Left: Structure of the cation in crystals of *trans*-[(Cl)Ru(py)$_4$(CO)](PF$_6$). Perspective view with thermal ellipsoids at the 30% probability level. Right: DFT optimized geometry for **[Ru-CO]$^+$** computed in vacuo.

However, since most of the experimental information discussed in this report deals with properties recorded in solution, we also performed geometry optimizations taking into account solvation effects by means of the PCM approximation. As evident in Table 3 this approach yielded essentially the same geometrical parameters. As typically observed with DFT at the level of theory employed in this report, the bond lengths are consistently overestimated, but the general structural features are well reproduced. For **[Ru-CO]$^+$** the computations predict a ν(CO) stretching frequency for at 1918 cm^{-1}, a value that agrees with the experimental one occurring at 1955 and 1960 cm^{-1} for solid samples and solutions in MeCN, respectively.

2.2. Donor/acceptor properties of the coordination sphere: electronic spectroscopy and electrochemical behavior

Fig. 3 displays the UV–Vis absorption spectra in MeCN. Absorption maxima and intensities for the transitions are listed in Table 4.

In spite of the structural similarities, the differences in the electronic spectra of the four species under consideration are evident. In general terms, the spectra display several features which appear to be compressed to the near UV end of the spectrum in **[Ru-NO]$^{2+}$**, widely spread into the visible region in **[Ru-Cl]^0**, and intermediately distributed in *trans*-[(Cl)Ru^{II}(py)$_4$(MeCN)]$^+$ (**[Ru-MeCN]$^+$**) and **[Ru-CO]$^+$**. This behavior can be rationalized in terms of the differential π-acceptor capabilities of the sixth ligand. Fig. 4 displays a comparative molecular-orbital (MO) diagram of the four species. The diagram reflects the splitting of the octahedral d_π (t_{2g}) set into *b* and *e* due to the lower C_4 symmetry of the molecule. The *e* set has the proper symmetry to become involved in π-interactions with the axial ligands. In all cases the coordinated chloride behaves as a π-donor ligand, while CH_3CN, CO and NO^+ are (in increasing order) efficient π-acceptor moieties. This interaction partially removes charge from the metal center stabilizing (in the expected order) the d_π orbitals but particularly those directly involved in the π-bonding. In this way, the electronic transitions shift to higher energies reflecting the stabilization of the metal d-orbitals.

The predicted (TD) DFT spectra for the four species agree nicely with the experimental ones and provide a tool to attempt a full spectral assignment. In the particular case of **[Ru-CO]$^+$**, whose spectrum is reported here for the first time, the features observed at 208, 232, and 264 nm arise from overlapping Ru(II) → π^*_{py} metal-to-ligand charge transfer (MLCT) transitions and $\pi_{py} \rightarrow \pi^*_{py}$ intraligand transitions. The lowest energy band at 302 nm (which has a noticeable tail to the low energy side, responsible for its pale yellow color in solution) are mostly Ru(II) → π^*_{py} in character. The computations also predict a weak Ru(II) → π^*_{CO} charge transfer at 280 nm, in a region dominated by much more intense transitions, precluding its direct observation and assignment.

The four species are electroactive in acetonitrile. The nitrosyl derivative displays a one-electron reduction process at −0.11 V, which has been ascribed to a ligand centered reduction to yield a {Ru-NO}^{7} species. Instead, **[Ru-Cl]^0** and **[Ru-MeCN]$^+$** can be reversibly oxidized at −0.16 and 0.58 V, respectively, in what has been described as a $Ru^{II/III}$ redox interconversion [4,20]. The cyclic voltammogram (CV) of **[Ru-CO]$^+$** in MeCN scanned towards anodic potentials shows a single quasi reversible wave at 1.39 V against Fc^+/Fc, independently of the scan rate. This signal is consistent with a 1-electron oxidation process, as also indicated by the controlled potential coulometry performed in the same medium. The recorded half wave potential for the oxidation process is considerably higher than the one reported for **[Ru-Cl]^0** and **[Ru-MeCN]$^+$** and is indicative of the much higher π-acceptor capability of CO if compared to Cl^- and MeCN. The increment in redox potential in this series of three compounds is higher than the predictions based on Lever parameters [30], also reflecting the π-acceptor nature of MeCN and CO. For completeness reasons, we report in depth on the spectral changes associated to the redox processes in

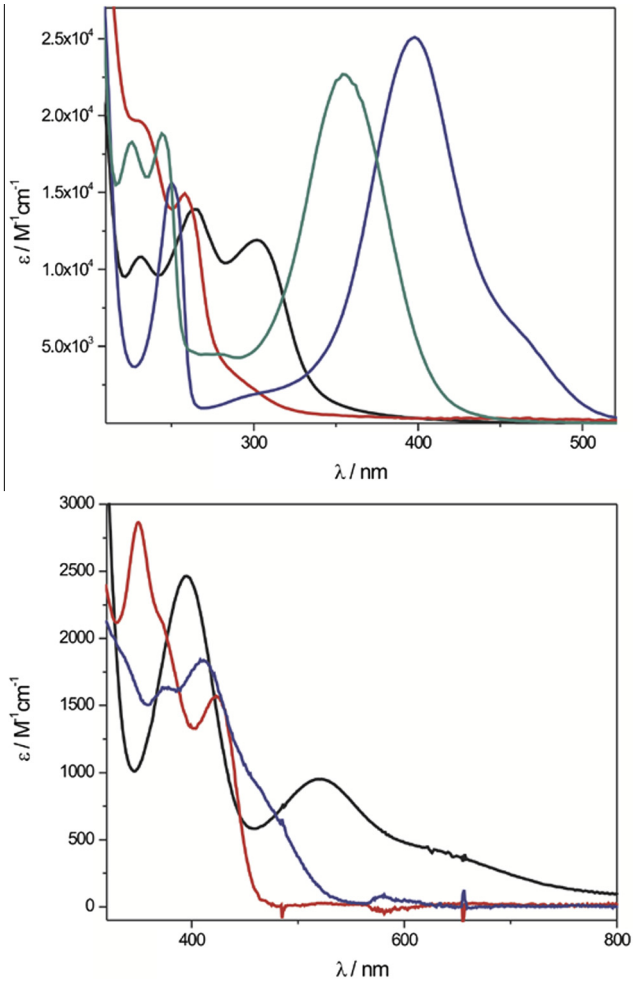

Fig. 3. Top: Electronic spectra of **[Ru-CO]$^+$** (black), **[Ru-NO]$^{2+}$** (red), **[Ru-Cl]^0** (blue) and **[Ru-MeCN]$^+$** (green) in acetonitrile. Bottom: Electronic spectra for **[Ru-CO]$^{2+}$** (black), **[Ru-Cl]$^+$** (blue) and **[Ru-MeCN]$^{2+}$** (red). (For interpretation of the references to colour in this figure legend, the reader is referred to the web version of this article.)

[Ru-CO]$^+$, **[Ru-Cl]^0** and **[Ru-MeCN]$^+$** in the supplementary information section of the manuscript. The analogous information for **[Ru-NO]$^{2+}$** has been reported by some of us elsewhere.

2.3. Reactivity

[Ru-Cl]^0 and **[Ru-MeCN]$^+$** do not undergo ligand substitution reactions at room temperature, but react readily in pyridine or ethanol under reflux in the presence of the appropriate entering group to yield symmetrically disubstituted tetrapyridine compounds [20,22,23,31]. On the contrary **[Ru-CO]$^+$** and **[Ru-NO]$^{2+}$** appear to be completely inert in solution. Every attempt to induce the thermal substitution of the chloride or the carbonyl moieties, ended up with essentially quantitative recovery of the starting material. Both species proved to be inert even when treated with Ag^+ [23]. This behavior does not parallel the observations in the related *cis*-$[(Cl)Ru(bpy)_2(NO)]^{2+}$ and *cis*-$[(Cl)Ru(bpy)_2(CO)]^+$, where only the nitrosyl derivative is inert, while *cis*-$[(Cl)Ru(bpy)_2(CO)]^+$ undergoes thermal chloride substitution [32], **[Ru-CO]$^+$**. The different reactivity compared to the bpy derivative is surprising, considering the fact that the Ru–Cl bond in the bipyridine based system is ca 0.045 Å shorter (d_{Ru-Cl} = 2.396(7) Å, d_{Ru-C} = 1.86(3) Å, d_{C-O} = 1.12(3) Å [32].

Photochemically, the situation is markedly different: upon irradiation, **[Ru-NO]$^{2+}$** undergoes an intramolecular electron transfer followed by ligand substitution, as represented above in Eq. (1), and has been thoroughly explored in this and other related systems. This behavior is not observed in the other members of this series not even the (also) strong acceptor carbonyl and is related to the non-innocent character of the nitrosyl ligand. Instead, solutions of **[Ru-CO]$^+$** exposed to light undergo ligand substitution reaction preserving the Ru(II) oxidation state. Fig. 5 displays the spectral changes observed upon irradiation of a *ca* 0.1 mM solution of **[Ru-CO]$^+$** in MeCN at 254 nm. The absorption bands at 232, 264 and 302 nm are gradually replaced by new ones at 244, and 353 nm, with isosbestic points at 252 and 319 nm. The presence of the latter suggests a clean conversion between **[Ru-CO]$^+$** and its photolysis product, without side reaction or further processes. The molar absorbance of the 353 nm band of the product, which is comparable to the one in **[Ru-MeCN]$^+$**, and the similarity of its

Table 4
Electronic spectra for **[Ru-CO]$^+$** and related species in acetonitrile.

	λ_{max}/nm (ε/10^3 M^{-1} cm^{-1})		λ_{max}/nm (ε/10^3 M^{-1} cm^{-1})
trans-$[(Cl)Ru(py)_4(CO)]^+$ (**[Ru-CO]$^+$**)	208 (21.2) 232 (10.8) 264 (13.9) 302 (11.9)	*trans*-$[(Cl)Ru(py)_4(CO)]^{2+}$ (**[Ru-CO]$^{2+}$**)	260 (15.7) 296 (6.4) 395 (2.4) 552 (0.9) 635 (0.4,sh)
trans-$[(Cl)Ru(py)_4(NO)]^{2+}$ [a] (**[Ru-NO]2+**)	230 (19.7) 258 (14.9) 288 (3.2, sh) 476 (0.2)		
trans-$(Cl)_2Ru(py)_4$ (**[Ru-Cl]^0**)	250 (15650) 398 (24991) 456 (6622,sh)	*trans*-$[(Cl)_2Ru(py)_4]^+$ (**[Ru-Cl]$^+$**)	263 (17.4) 350 (2.8) 368 (2.2, sh) 424 (1.5)
trans-$[(Cl)Ru(py)_4(MeCN)]^+$ [b] (**[Ru-MeCN]$^+$**)	226 (17.8) 246 (18.1) 355 (22.1)	*trans*-$[(Cl)Ru(py)_4(MeCN)]^{2+}$ [b] (**[Ru-MeCN]$^{2+}$**)	255 (24.1) 328 (1.9, sh) 375 (1.7, sh) 410 (1.8) 458 (0.9)
trans-$[(Cl)Ru(py)_3(MeCN)_2]^+$ *trans*-$[(Cl)Ru(py)_2(MeCN)_3]^+$ *trans*-$(Cl)_2Ru(py)_3(MeCN)$ *trans*-$(Cl)_2Ru(py)_2(MeCN)_2$	340 (15.6) 332 (74.4) 380 (16.2) 356 (5.9) 408 (1.5,sh)		

[a] From Ref. [27].
[b] Form Ref. [20].

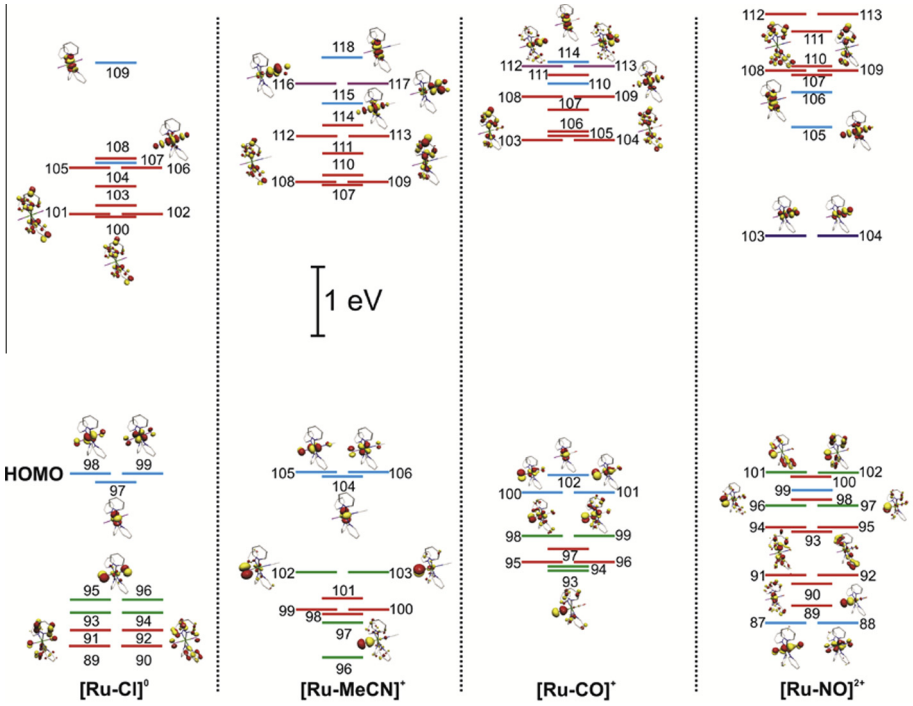

Fig. 4. Molecular orbital diagram for **[Ru-CO]⁺** and related species. All the orbital energies are referred to the one of HOMO. Orbitals are color-coded according to their assignment as metal-centered (blue), pyridine-centered (red) or chloride-centered (green). The ones represented in violet for **[Ru-MeCN]⁺**, **[Ru-CO]⁺** and **[Ru-NO]²⁺** are mostly MeCN, CO or NO^+ in character, respectively. (For interpretation of the references to colour in this figure legend, the reader is referred to the web version of this article.)

overall spectrum with the one of **[Ru-MeCN]⁺** suggests that the tetrakis-pyridine moiety is preserved and a carbonyl molecule is released along the photo-reaction.

To asses this assignment, we preformed complementary experiments at higher concentration, which allow following the reaction with more specific spectroscopies, namely IR and ^{1}H NMR (see Fig. 6). The interaction with light yields a species whose vibrational spectrum lacks from any signals arising from carbonyl centered vibrations. Along the experiment, the growth of a weak signal at 2136 cm^{-1} seems to indicate the presence of free carbon monoxide (ν(CO(g)) = 2138 cm^{-1}) [33]. Both results support our previous interpretation in terms of the release of a CO molecule. The ^{1}H NMR spectrum of the photolysis product is virtually indistinguishable from the one obtained from a pure sample of **[Ru-MeCN]⁺**, confirming that the first process is best described by Eq. (4):

$$trans\text{-}[(Cl)Ru^{II}(py)_4(CO)]^+ \xrightarrow[MeCN]{h\nu} trans\text{-}[(Cl)Ru^{II}(py)_4(MeCN)]^+ + CO \quad (4)$$

Further irradiation under NMR conditions of the **[Ru-MeCN]⁺** generated in Eq. (4) reveals the formation of free pyridine and a parallel growth of an equal amount of a pyridine holding species, which can be formulated as $[(Cl)Ru^{II}(py)_3(MeCN)_2]^+$:

$$trans\text{-}[(Cl)Ru^{II}(py)_4(MeCN)]^+ \xrightarrow[MeCN]{h\nu} [(Cl)Ru^{II}(py)_3(MeCN)_2]^+ + py \quad (5)$$

Complemetary experiments irradiating a pure sample of **[Ru-MeCN]⁺** under NMR conditions in CD_3CN, allow exploring the photoinduced exchange of the coordinated MeCN. The spectra recorded in the dark show no exchange with the solvent for periods of several hours. On the contrary, upon irradiation the spectra show substantial lowering of the signals due to coordinated MeCN even at short time of photolysis without any detectable changes in the aromatic region. This result suggests that reaction (5) competes with the photoinduced exchange of MeCN, a process that remains undetectable under UV–Vis conditions even being much faster than the loss of pyridine.

Irradiation at λ_{irr} = 254 nm in *diluted* solutions of **[Ru-CO]⁺** does not show any evidence of photodecomposition of the formed **[Ru-MeCN]⁺**. This behavior is a simple consequence of the low extinction coefficient of the latter at this particular wavelength, making reaction 5 extremely inefficient in the presence of unreacted **[Ru-CO]⁺**, unless high concentrations are employed. Eventually, the photolysis of *pure and diluted* solutions of **[Ru-MeCN]⁺** lead the expected pyridine loss to yield $[(Cl)Ru^{II}(py)_3(MeCN)_2]^+$. In the electronic spectrum this is revealed by the appearance of an absorption band at higher energy (λ_{max} = 340 nm) and markedly lower intensity ($\varepsilon = 15.6 \times 10^3\ M^{-1}\ cm^{-1}$). This behavior is not privative of **[Ru-MeCN]⁺**: Fig. 7 also shows similar spectral changes in the photolysis of **[Ru-Cl]⁰**, suggesting that also in this case the substitution of one pyridine molecule by MeCN is preferred over the chloride loss to yield a species that can be formulated as $(Cl)_2Ru^{II}(py)_3(MeCN)$:

$$trans\text{-}(Cl)_2Ru^{II}(py)_4 \xrightarrow[MeCN]{h\nu} (Cl)_2Ru^{II}(py)_3(MeCN) + py \quad (6)$$

Both $[(Cl)Ru^{II}(py)_3(MeCN)_2]^+$ and $(Cl)_2Ru^{II}(py)_3(MeCN)$ proved to be photoactive. The spectral changes upon irradiation (shifts of the absorption maxima to lower wavelengths, lower extinction coefficients of the products) are again compatible with to loss of pyridine molecules to yield $[(Cl)Ru^{II}(py)_2(MeCN)_3]^+$ and $(Cl)_2Ru^{II}(py)_2(MeCN)_2$, respectively:

$$[(Cl)Ru^{II}(py)_3(MeCN)_2]^+ \xrightarrow[MeCN]{h\nu} [(Cl)Ru^{II}(py)_2(MeCN)_3]^+ + py \quad (7)$$

$$(Cl)_2Ru^{II}(py)_3(MeCN) \xrightarrow[MeCN]{h\nu} (Cl)_2Ru^{II}(py)_2(MeCN)_2 + py \quad (8)$$

When diluted solutions of **[Ru-CO]⁺** are irradiated at other wavelengths, the overall products seem to be the same as those described above for 254 nm. However, due to the fact that the

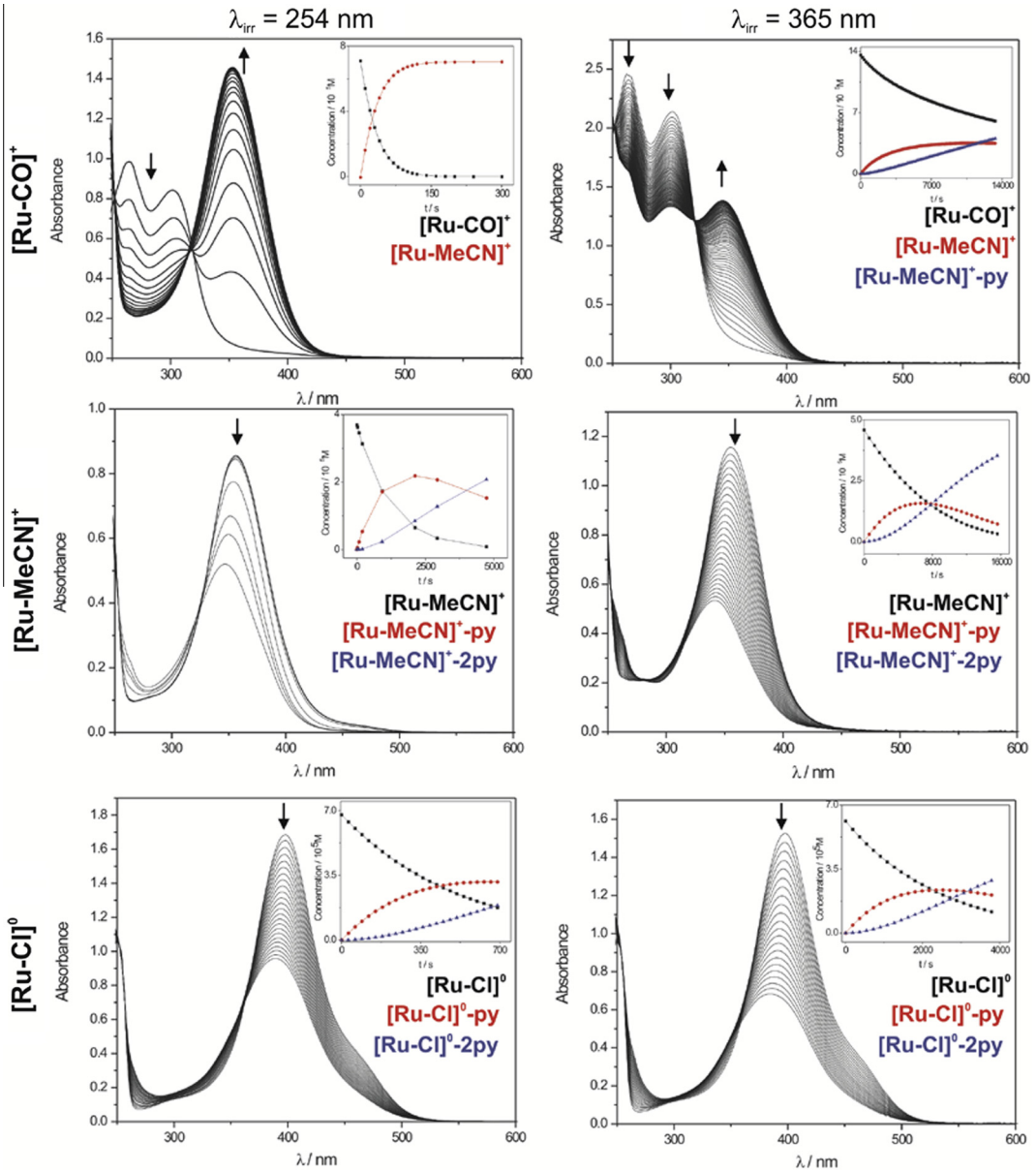

Fig. 5. Spectral changes along the irradiation of **[Ru-CO]$^+$**, **[Ru-MeCN]$^+$** and **[Ru-Cl]^0** in MeCN, λ_{irr} = 254 nm (left) and 365 nm (right). See the experimental section for details. The arrows indicate the spectral changes along the irradiation time. The insets represent the fraction of the different species present in solution as obtained from the global analysis. **[Ru-MeCN]$^+$-py**, **[Ru-MeCN]$^+$-2py**, **[Ru-Cl]^0-py** and **[Ru-Cl]^0-2py** stand for *trans*-$[(Cl)Ru^{II}(py)_3(MeCN)_2]^+$, $[(Cl)Ru^{II}(py)_2(MeCN)_3]^+$, $(Cl)_2Ru^{II}(py)_3(MeCN)$ and $(Cl)_2$-$Ru^{II}(py)_2(MeCN)_2$, respectively.

ratios of molar absorptivities between **[Ru-CO]$^+$** and **[Ru-MeCN]$^+$** are dependent on the λ_{irr}, the photo-process might lead markedly different concentration profiles of the reaction products. For instance, when submilimolar solutions of **[Ru-CO]$^+$** are irradiated with higher wavelength light (365 nm) the global analysis suggests the presence of three colored species, in agreement with two consecutive processes. The analysis also shows that the only colored species present in these solutions along the photolysis are **[Ru-CO]$^+$**, **[Ru-MeCN]$^+$** and $[(Cl)Ru^{II}(py)_3(MeCN)_2]^+$. A quantitative treatment of the spectral evolution allows determining the quantum yields associated with the different photo-processes (ϕ_A and ϕ_B). A multiwavelength spectral approach, where the fraction of light absorbed by the different species at λ_{irr} was properly acquainted for, yielded the values shown in Table 5.

A global inspection of the qualitative information described above and the quantitative data contained in Table 5 render a few general observations concerning the photochemical behavior in MeCN. (1) There is no evidence showing the photo-release of a chloride anion in none of the molecules under study: in all cases, the preferred process seems to involve the photosubstitution of neutral carbonyl of pyridine molecule from the coordination sphere. (2) When available, the photo-release of CO in **[Ru-CO]$^+$** and MeCN in **[Ru-MeCN]$^+$** is favored over the substitution of a pyridine molecule, $\phi_{\text{-CO}}$ and $\phi_{\text{-MeCN}}$ being always larger than $\phi_{\text{-py}}$, no matter the composition of the rest of the coordination sphere. (3) The quantum yields for the different processes are not markedly dependent on λ_{irr}. The largest ration actually corresponds to the photo-liberation of CO in **[Ru-CO]$^+$**, but even in this case the difference is less than one order of magnitude. At this point it is not clear why Cl^- is never released as well the reasons behind the exclusive dissociation of a CO molecule form **[Ru-CO]$^+$**. The DFT computed geometry of the lowest energy triplet excited-state in **[Ru-CO]$^+$**,

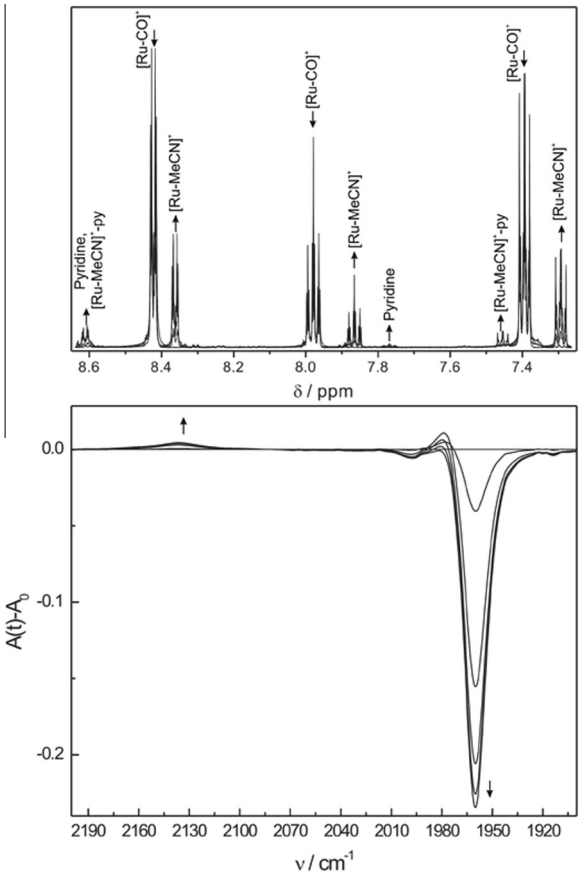

Fig. 6. NMR Spectral changes (top) and IR Spectral changes (bottom) along the irradiation of **[Ru-CO]$^+$** in MeCN, λ_{irr} = 254 nm. See the experimental section for details. **[Ru-MeCN]$^+$-py** stands for $[(Cl)Ru^{II}(py)_3(MeCN)_2]$.

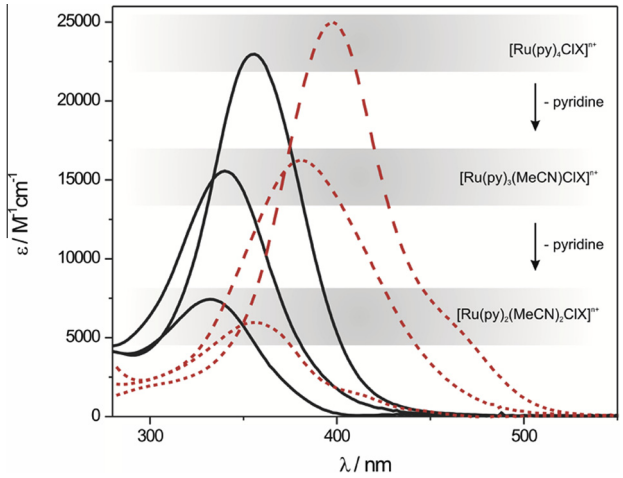

Fig. 7. Electronic spectra for **[Ru-MeCN]$^+$** (X = MeCN, red dotted lines) and **[Ru-Cl]^0** (X = Cl^-, black full lines) and their photoproducts. (For interpretation of the references to colour in this figure legend, the reader is referred to the web version of this article.)

presumably involved in the photo-detachment of CO, certainly reveals a substantial weakening of the Ru–CO bond, but the same could be said about the average Ru–py bond length. This effect arises from the fact that this excited state is d-d in nature. The anti-bonding nature of the e_g^* orbitals that become populated in this state is responsible for the expansion of the coordination sphere.

Table 5
Quantum yields for the photo-processes described in the text.

	λ = 254 nm	λ = 365 nm
[Ru-CO]$^+$	$\phi_A = 1.8 \times 10^{-1}$	$\phi_A = 2.7 \times 10^{-2}$; $\phi_B = 2.1 \times 10^{-3}$
[Ru-MeCN]$^+$	$\phi_A = 4.8 \times 10^{-3}$; $\phi_B = 1.5 \times 10^{-3}$	$\phi_A = 2.0 \times 10^{-3}$; $\phi_B = 6.0 \times 10^{-3}$
[Ru-Cl]^0	$\phi_A = 1.2 \times 10^{-2}$; $\phi_B = 8.0 \times 10^{-3}$	$\phi_A = 1.3 \times 10^{-2}$; $\phi_B = 1.0 \times 10^{-2}$

However this electronic picture by itself cannot account for the inertness of the Ru–py or Ru–Cl bond in **[Ru-CO]$^+$**. We can only speculate that the recombination of a potentially detached py or Cl^- ligand within the solvent cage (or alternatively the escape of the CO fragment from the same cage) is favored.

3. Conclusions

We have successfully explored the photochemistry in solution of a series of simple mononuclear tetrakis-pyridine ruthenium (II) species, including the preparation and isolation of *trans*-$[(Cl)Ru(py)_4(CO)](PF_6)$, which was fully characterized employing X-ray diffraction techniques, providing structural information of a π-acceptor holding system that complements the many reports on the isoelectronic *trans*-$[(Cl)Ru(py)_4(NO)]^{3+}$ cation. The experimental data was complemented with electronic structure computations for these compounds in both $Ru^{II/III}$ oxidation states, providing a rationale for the trends in the different experimental properties.

The three *trans*-$[(Cl)Ru(py)_4(CO)]^+$, *trans*-$(Cl)_2Ru(py)_4$ and *trans*-$[(Cl)Ru(py)_4(MeCN)]^+$ turned out to be undergo ligand substitution reactions under photolysis. In all cases the processes are not simple, involving the consecutive loss of CO, MeCN or pyridine ligands. Based on a multiwavelength treatment of the absorption profile along the photolysis experiments, we provide reliable quantitative values for the quantum yields of the different photo-processes. In all cases the numerical values are high enough so as to observe changes in reasonably short periods of time without the need of high power light sources. The overall numbers are smaller than those collected in the $\{Ru(bpy)_2\}^{2+}$ systems. Nevertheless, the $\{Ru(py)_4\}^{2+}$ systems tend to display much higher extinction coefficients than the polypyridine ones [26], therefore these results suggest that, unlike what is usually assumed in the literature, photochemistry might become a complication when employing these systems as building blocks of larger molecular arrangements.

4. Experimental

4.1. Synthesis of the compounds

The compounds *trans*-$Ru(Cl)_2(py)_4$, *trans*-$[(Cl)Ru(py)_4(NO)](PF_6)_2$ and *trans*-$[(Cl)Ru(py)_4(MeCN)](PF_6)$ were prepared according to previously published procedures [9,20] and fully characterized by IR (KBr pellets), ^1H- and ^{13}C NMR spectroscopies and elemental analyses. Carbon monoxide was synthesized by the reaction of sulfuric and formic acid. All other reagents employed in this work were obtained commercially and used as supplied.

***trans*-[(Cl)Ru(py)$_4$(CO)](PF$_6$), [Ru-CO](PF$_6$)** *trans*-$[(Cl)Ru^{II}(py)_4(NO)](PF_6)_2$ (193.0 mg, 0.285 mmols) and NaN_3 (16.1 mg, 0.285 mmols) were allowed to react two hours in acetone (5 mL) under argon atmosphere and protected from the light to yield the solvento complex *trans*-$[(Cl)Ru(py)_4(Me_2CO)]^+$ as previously reported by Coe and coworkers [23]. The system was then frozen with liquid nitrogen and the gas phase was evacuated in order to

replace it by CO gas. The mixture was left at room temperature for 24 h, and the solution turned from dark orange to yellow. The solution was then concentrated to *ca.* 2 mL and precipitation of the product was induced by addition of diethylether (10 mL). The yellow solid was collected by filtration, washed with diethylether and dried under vacuum. Yield: 123 mg (62% based on *trans*-[(Cl)Ru(py)$_4$(CO)](PF$_6$)). Further purification was achieved by slow diffusion of diethylether onto a concentrated MeCN solution of the compound. Yield: 69 mg. *Anal.* Calc. for $C_{21}H_{20}F_6Cl_1N_4O_1P_1Ru_1$ (MW = 625.90): C, 40.27; H, 3.22; N, 8.95. Found: C, 40.8; H, 3.2; N, 8.8%. ^{1}H NMR: δ_H (CD_3CN): 8.42 (8H, d, $H^{2,6} \times 4$), 7.98 (4H, t, $H^4 \times 4$), 7.40 (8H, t, $H^{3,5} \times 4$). ^{13}C NMR: δ_C (CD_3CN): 199 (1C, $C^{11} \times 1$), 156.1 (8C, $C^{2,6} \times 4$), 138.85 (4C, $C^4 \times 4$), 125.79 (8C, $C^{3,5} \times 4$). IR(KBr): ν(CO) 1955 cm^{-1}.

4.2. Physical determinations

Microanalytical data for C, H and N were obtained with a Carlo Erba EA 1108 analyzer. UV–Vis spectra were recorded with either an HP8453 or an HP8452A diode array spectrophotometer. IR spectral measurements (KBr pellets) were carried out using a Nicolet iS10. The ^{1}H and ^{13}C NMR spectra were measured with a 500 MHz Bruker AM 500 spectrometer; chemical shifts are referred to TMS. Cyclic Voltammetry (CV) measurements in MeCN employing 0.1 M Bu_4NPF_6 as supporting electrolyte were performed with a standard three electrode cell containing a working vitreous carbon electrode (3 mm Ø), a Pt wire as a counter electrode, and a silver wire plus an internal ferrocene (Fc) standard as a reference. The potential of the working electrode was controlled by a TEQ-03 potentiostat.

The spectroelectrochemical and coulometric experiments were done under argon in 0.2 M $TBAPF_6$ MeCN solutions. **[Ru-CO]$^+$** was alternatively oxidized and reduced at −16 °C under controlled potential conditions. The infrared spectroelectrochemical experiments were performed using a three-electrode OTTLE cell [34]. For the UV–Vis spectroelectrochemistry, a specially modified 1-cm path length quartz cuvette attached to a 5-mL glass container was used. The whole setup was purged with Ar and temperature controlled (Lauda RL6 CP cryostat). Electrolysis was performed over a platinum mesh. A second platinum grid separated by a frit glass was used as a counter electrode, and Ag/$AgNO_3$ (0.01 M in MeCN) was used as a reference.

Photochemical experiments were performed employing a 365 nm Ligh Emitting Diode and a 254 nm lamp (Philips TUV 4 W T5 lamp). The intensity of the 365 nm LED and the 254 nm lamp (2.44×10^{-6} and 1.5×10^{-5} einstein s^{-1} dm^{-3}, respectively) were determined by reference to a 450 nm LED source employing a FieldMaster-Coherent power meter with a LM-2UV photodiode as light sensor. The 450 nm LED was calibrated by actinometry employing a standard solution of *cis*-[Ru(bpy)$_2$(py)$_2$]$^{2+}$ (quantum yield of photosubstitution = 0.26) [35], yielding an intensity of 3.61×10^{-6} einstein s^{-1} dm^{-3}.

The quantum yields for the photoprocesses discussed in this work were determined spectrophotometrically by measuring the spectral changes along the irradiation time under medium-to-high conversion conditions. As a starting point, the analysis requires an accurate estimation of the number of colored species, which in our case was performed by factor analysis [36]. Depending on the experiment we found two or three colored species in solution. The former situation indicates a simple A → B conversion between the reactant and the product, and was modeled with the following set of equations, where all the symbols have their usual meaning:

$$-\frac{dc_A}{dt} = \frac{dc_B}{dt} = I_A \phi_A \tag{9}$$

$$I_A = I_0 f_A \left(1 - 10^{-\sum \varepsilon_i b c_i}\right) \tag{10}$$

$$f_A = \frac{\varepsilon_A b c_A}{\sum \varepsilon_i b c_i} \tag{11}$$

The factor f_A was introduced to take into account the actual fraction of light absorbed by the reactant. The presence of a third colored species is the signature of two consecutive photochemical events (A → B → C). The rate of change of the different species in solution was modeled using the following set of equations.

$$-\frac{dc_A}{dt} = I_A \phi_A; \quad \frac{dc_B}{dt} = I_A \phi_A - I_B \phi_B; \quad \frac{dc_C}{dt} = I_B \varphi_B \tag{12-14}$$

$$f_j = \frac{\varepsilon_j b c_j}{\sum \varepsilon_i b c_i} \tag{15}$$

$$I_j = I_0 f_j (1 - 10^{-\sum \varepsilon_i b c_i}) \tag{16}$$

The equations were solved numerically. The quantum yields for the different processes where obtained by scanning ϕ_A (an ϕ_B) in the [0,1] range. A multiwavelength treatment of the absorption profiles rendered the spectra of all the species involved in the processes.

4.3. X-ray crystallographic data collection and refinement of the structures

A 0.26 × 0.24 × 0.23 mm single crystal of **[Ru-CO]**(PF$_6$) was coated with perfluoropolyether, picked up with nylon loops and mounted in the nitrogen cold stream a Bruker AXS Kappa Mach3/APEX II diffractometer equipped with a Mo-target rotating-anode X-ray source and INCOATEC Helios Mirror X-ray optics (λ = 0.71073 Å). Final cell constants were obtained from least squares fits of several thousand strong reflections. Intensities of redundant reflections were used to correct for absorption using the program SADABS [37]. The structures were readily solved by Patterson methods and subsequent difference Fourier techniques. The Siemens ShelXTL [38] software package was used for solution and artwork of the structures and ShelXL-2013 [39] was used for structure refinement. All non-hydrogen atoms were anisotropically refined and hydrogen atoms bound to carbon were placed at calculated positions and refined as riding atoms with isotropic displacement parameters.

4.4. Theoretical calculations

We employed Density Functional Theory (DFT) computations to fully optimize the geometries of the ground states of *trans*-[(Cl)Ru(py)$_4$(CO)]$^{+/2+}$, *trans*-[(Cl)Ru(py)$_4$(NO)]$^{2+}$, *trans*-[(Cl)$_2$Ru(py)$_4$]$^{0/+}$ and *trans*-[(Cl)Ru(py)$_4$(MeCN)]$^{+/2+}$ in vacuum and considering solvation effects by means of the PCM approximation. The calculations were carried out with the GAUSSIAN *03* package [40], without symmetry constraints using Becke's three parameter hybrid functional with the correlation functional of Lee, Yang and Parr formalized as the B3LYP hybrid functional [41–44] and the effective core potential basis set LanL2DZ [45–47], which proved to be suitable for geometry predictions in coordination compounds containing metals of the second row of the transition elements in the Periodic Table. We used tight SCF convergence criteria and default settings in the geometry optimizations and restricted and unrestricted approximations of the Kohn–Sham equations, depending on the total number of electrons [48]. The true nature of the stationary points, which correspond to (local) minima in the potential energy surface, was confirmed by numerical vibrational frequency computations. In all cases the absence of negative

frequencies confirmed that the optimized geometries correspond to stable configurations in the potential energy surfaces. Time dependent (TD)DFT computations at the ground state equilibrium geometry involving 100 singlet states for *trans*-$[(Cl)Ru(py)_4(CO)]^+$, *trans*-$[(Cl)Ru(py)_4(NO)]^{2+}$, *trans*-$[(Cl)_2Ru(py)_4]^0$ and *trans*-$[(Cl)Ru(py)_4(MeCN)]^+$ and 100 doublets for *trans*-$[(Cl)Ru(py)_4(CO)]^{2+}$, *trans*-$[(Cl)_2Ru(py)_4]^+$ and *trans*-$[(Cl)Ru(py)_4(MeCN)]^{2+}$ were employed as an assistant tool in the interpretation and assignment of the electronic spectra and photochemical properties.

4.5. Supporting information available

IR and NMR spectra of **[Ru-CO]$^+$**; spin density for **[Ru-NO]$^{2+}$**, **[Ru-Cl]$^+$** and **[Ru-MeCN]$^{2+}$**; DFT computed MO orbitals and (TD)DFT electronic transitions for **[Ru-CO]$^{+/2+}$**, **[Ru-NO]$^{2+}$**, **[Ru-Cl]$^{0/+}$** and **[Ru-MeCN]$^{+/2+}$**, Molecular Orbital Diagram for **[Ru-CO]$^{2+}$**, **[Ru-Cl]$^+$** and **[Ru-MeCN]$^{2+}$**; UV–Vis and IR spectroelectrochemistry for **[Ru-CO]$^+$/[Ru-CO]$^{2+}$** conversion (34 pages).

Acknowledgements

This work has been supported by grants from CONICET, ANPCyT, the University of Buenos Aires, and the National Center for Supercomputing Applications (grant TG-MCA05S010). LDS is a member of the scientific staff of CONICET. JPM is a doctoral fellow of the same Institution. The authors wish to thank Dr. G. Pieslinger for providing access to a pure sample of **[Ru-MeCN]$^+$**, as well as for his advice concerning the storage and manipulation of this material.

Appendix A. Supplementary material

CCDC 1008214 contain the supplementary crystallographic data for this paper. These data can be obtained free of charge from The Cambridge Crystallographic Data Centre via www.ccdc.cam.ac.uk/data_request/cif. Supplementary data associated with this article can be found, in the online version, at http://dx.doi.org/10.1016/j.ica.2014.12.039.

References

[1] E.W. Abel, M.A. Bennett, G. Wilkinson, J. Chem. Soc. (1959) 3178.
[2] F. Bottomley, E. Hahn, J. Pickardt, H. Schumann, M. Mukaida, H. Kakihana, J. Chem. Soc., Dalton Trans. (1985) 2427.
[3] J.D. Gilbert, D. Rose, G. Wilkinson, J. Chem. Soc. A (1970) 2765.
[4] F. Bottomley, P.S. White, M. Mukaida, K. Shimura, H. Kakihana, J. Chem. Soc., Dalton Trans. (1988) 1965.
[5] Z. Bu, Z. Wang, L. Yang, S. Cao, Appl. Organomet. Chem. 24 (2010) 813.
[6] J. Chen, L. Han, Z. Chen, Acta Crystallogr., Sect. E 58 (2002) m588.
[7] B. Cormary, I. Malfant, M. Bouron-Le Cointe, L. Toupet, B. Delley, D. Schaniel, D. Mockus, T. Woike, K. Fejfarova, V. Petricek, M. Dusek, Acta Crystallogr., Sect. B 65 (2009) 612.
[8] P. Desjardins, G.P.A. Yap, R.J. Crutchley, Inorg. Chem. 38 (1999) 5901.
[9] T. Kimura, T. Sakurai, M. Shima, T. Togano, M. Mukaida, T. Nomura, Inorg. Chim. Acta 69 (1983) 135.
[10] H. Nagao, K. Aoyagi, Y. Yukawa, F.S. Howell, M. Mukaida, H. Kakihana, Bull. Chem. Soc. Jpn. 60 (1987) 3247.
[11] H. Nishimura, H. Matsuzawa, T. Togano, M. Mukaida, H. Kakihana, F. Bottomley, J. Chem. Soc., Dalton Trans. (1990) 137.
[12] J.L. Templeton, J. Am. Chem. Soc. 101 (1979) 4906.
[13] X. Wu, R. Ye, A. Jia, Q. Chen, Q. Zhang, Acta Crystallogr., Sect. E 69 (2013) m105.
[14] Y. Yukawa, K. Aoyagi, M. Kurihara, K. Shirai, K. Shimizu, M. Mukaida, T. Takeuchi, H. Kakihana, Chem. Lett. (1985) 283.
[15] Y. Zhou, H. Xiao, L. Kang, J. Zuo, C. Li, X. You, Dalton Trans. (2009) 10256.
[16] B. Cormary, S. Ladeira, K. Jacob, P.G. Lacroix, T. Woike, D. Schaniel, I. Malfant, Inorg. Chem. 51 (2012) 7492.
[17] P.T. Cheng, B.R. Loescher, S.C. Nyburg, Inorg. Chem. 10 (1971) 1275.
[18] H.A. Mirza, A.A. Farah, D.V. Stynes, A.B.P. Lever, Acta Crystallogr. Sect. E 59 (2003) m679.
[19] P. Albores, L.D. Slep, T. Weyhermuller, L.M. Baraldo, Inorg. Chem. 43 (2004) 6762.
[20] G.E. Pieslinger, P. Albores, L.D. Slep, B.J. Coe, C.J. Timpson, L.M. Baraldo, Inorg. Chem. 52 (2013) 2906.
[21] Y.S. Varshavsky, T.G. Cherkasova, M.R. Galding, V.N. Khrustalev, I.S. Podkorytov, V.A. Gindin, S.N. Smirnov, A.B. Nikol'skii, J. Organomet. Chem. 694 (2009) 2917.
[22] B.J. Coe, T.J. Meyer, P.S. White, Inorg. Chem. 34 (1995) 3600.
[23] B.J. Coe, T.J. Meyer, P.S. White, Inorg. Chem. 34 (1995) 593.
[24] P. Albores, L.D. Slep, L.S. Eberlin, Y.E. Corilo, M.N. Eberlin, G. Benitez, M.E. Vela, R.C. Salvarezza, L.M. Baraldo, Inorg. Chem. 48 (2009) 11226.
[25] F. Roncaroli, M.E. Ruggiero, D.W. Franco, G.L. Estiu, J.A. Olabe, Inorg. Chem. 41 (2002) 5760.
[26] A. Juris, V. Balzani, F. Bariglietti, S. Campagna, P. Belser, A. von Zelewsky, Coord. Chem. Rev. 84 (1988) 85.
[27] A.G. De Candia, J.P. Marcolongo, R. Etchenique, L.D. Slep, Inorg. Chem. 49 (2010) 6925.
[28] M.R.J. Elsegood, D.A. Tocher, Acta Crystallogr., Sect. C 51 (1995) 40.
[29] N.S. Al-Zamil, E.H.M. Evans, R.D. Gillard, D.W. James, T.E. Jenkins, R.J. Lancashire, P.A. Williams, Polyhedron 1 (1982) 525.
[30] A.B.P. Lever, Inorg. Chem. 29 (1990) 1271.
[31] F. Bottomley, M. Mukaida, J. Chem. Soc., Dalton Trans. (1982) 1933.
[32] J.M. Clear, J.M. Kelly, C.M. O'Connell, J.G. Vos, C.J. Cardin, S.R. Costa, A.J. Edwards, J. Chem. Soc. Chem. Comm. (1980) 750.
[33] K. Nakamoto, Infrared and Raman Spectra of Inorganic and Coordination Compounds, John Wiley & sons, New York, 1986.
[34] M. Krejcik, M. Danek, F. Hartl, J. Electroanal. Chem. 317 (1991) 179.
[35] D.V. Pinnick, B. Durham, Inorg. Chem. 23 (1984) 1440.
[36] E.R. Malinovsky, Factor Analysis in Chemistry, Wiley-Interscience, New York, 1991.
[37] SADABS, Bruker AXS Inc., Madison, WI, USA, 2007.
[38] ShelXTL, Bruker AXS Inc., Madison, WI, USA, 2003.
[39] G.M. Sheldrick, Acta Crystallogr., Sect. A 64 (2008) 112.
[40] M.J. Frisch et al., Gaussian Inc., Wallingford, CT, 2004.
[41] A.D. Becke, J. Chem. Phys. 84 (1988) 4524.
[42] A.D. Becke, J. Chem. Phys. 98 (1993) 5648.
[43] C. Lee, W. Yang, R.G. Parr, Phys. Rev. B 37 (1988) 785.
[44] J.P. Perdew, Phys. Rev. B 33 (1986) 8822.
[45] T.H. Dunning Jr., P.J. Hay, in: H.F. Schaefer III (Ed.), Modern Theoretical Chemistry, Plenum, New York, NY, 1976, p. 1.
[46] P.J. Hay, W.R. Wadt, J. Chem. Phys. 82 (1985) 270.
[47] P.J. Hay, W.R. Wadt, J. Chem. Phys. 82 (1985) 299.
[48] J. Li, L. Noodleman, D.A. Case, in: E.I. Solomon, A. P.B. Lever, (Eds.), Inorganic Electronic Structure and Spectroscopy, vol. 1, Wiley, 1999, p. 661.